Basin Research (1999) **11,** 205–221

Sedimentation and deformation in a Pliocene–Pleistocene transtensional supradetachment basin, Laguna Salada, north-west Mexico

R. Dorsey* and A. Martín-Barajas†

Department of Geological Sciences, 1272 University of Oregon, Eugene, OR 97403–1272, USA
†Departamento de Geología, Centro de Investigación Científica y de Educación Superior de Ensenada, Baja California, Mexico

ABSTRACT

This study examines a thick section of Pliocene–Pleistocene sedimentary rocks exposed in the footwall of an active normal fault (Cañon Rojo fault) near its intersection with the dextral-normal Laguna Salada fault in north-western Mexico. These rocks are situated in the upper plate of an inactive strand of the Cañada David detachment fault, which is cut on the north-east by the Laguna Salada fault. The stratigraphy is divided into three unconformity-bounded sequences: (1) marine mudstone of the Pliocene Imperial Formation; (2) nonmarine Pliocene–Pleistocene redbeds, consisting of sedimentary breccia, conglomerate, conglomeratic sandstone (all un-named) and fine-grained sandstone and mudstone of the Palm Spring Formation; and (3) uncemented Pleistocene boulder gravel. Coarse deposits of the redbeds sequence were deposited in fault-bounded, high- and low-gradient alluvial fans that passed laterally into a low-energy fluvial plain of the ancestral Colorado River (Palm Spring Formation) which occupied the present-day Laguna Salada.

Detailed mapping reveals convergence and lap-out of bedding surfaces in the redbeds sequence onto the west limb of a large anticline cored by Imperial Formation. These geometries, combined with fanning dips and thickening of stratigraphy into the flanking syncline, indicate that the anticline grew during deposition of the redbeds. Fold axes of the growth anticline and smaller related folds trend N to NNE, parallel to the strike of associated normal faults and perpendicular to the extension direction. Based on its orientation, large size and relationship to neighbouring structures, the anticline is interpreted to be a fault-bend fold that grew in response to slip of the upper plate over a bend in the Cañada David detachment fault during deposition in a transtensional supradetachment basin. Localized subsidence in the flanking syncline resulted in deposition of >1000 m of alluvial sediments near its intersection with the Laguna Salada fault. Sedimentary detritus is derived exclusively from the north-east (footwall) side of the dextral-normal Laguna Salada fault, indicating that topographic relief was high in the Sierra Cucapa and was subdued or negligible in the footwall of the coeval Cañada David detachment. Following deposition of the redbeds and grey gravel units, the northern part of the detachment fault was abandoned and the modern Cañon Rojo fault was initiated, producing rapid footwall uplift and erosion of previously buried stratigraphy. Slip rate on the Cañon Rojo fault is estimated to be ≈ 2–4 mm yr^{-1} since middle Pleistocene time, similar to the late Pleistocene to Holocene rate determined in previous studies.

INTRODUCTION

Sedimentation in active extensional and strike-slip basins is characterized by steep depositional gradients, dynamic interplay between fault-controlled subsidence and sediment accumulation, and abrupt lateral changes from coarse basin-margin deposits to fine-grained axial facies (Crowell & Link, 1982; Christie-Blick & Biddle, 1985; Leeder & Gawthorpe, 1987; Frostick & Steel, 1993). Extensional basins may form by high-angle rifting in areas of normal heat flow and relatively slow fault slip rates, or by low-angle detachment faulting in regions of high heat flow and rapid, high-magnitude extension (Friedmann & Burbank, 1995). Strike-slip basins may be

either transtensional or transpressional in nature, with transtensional basins forming by subsidence on normal and oblique-normal faults that form in releasing bends and step-overs of strike-slip fault zones (e.g. Christie-Blick & Biddle, 1985; Mann, 1997). Recent studies have recognized the importance of kinematic connections between low-angle detachment faults and strike-slip faults in zones of transtensional deformation (e.g. Burchfiel *et al.*, 1987; Oldow *et al.*, 1994), which may result in formation of transtensional supradetachment basins (Dinter & Royden, 1993; May *et al.*, 1993; Burchfiel *et al.*, 1995). Patterns of sedimentation and syndepositional deformation in such basins are likely to be complicated due to the large variety of extensional, strike-slip, and oblique-slip faults and related folds that are expected to influence the basin and its margins during subsidence and filling. Transtensional supradetachment basins have only recently been recognized as an important component of strike-slip fault systems, and therefore detailed aspects of their sedimentation and deformation histories remain poorly understood.

This paper presents the results of an integrated sedimentological, stratigraphic and structural study of Pliocene–Pleistocene alluvial-fan deposits that accumulated in a transtensional supradetachment basin within the strike–slip plate boundary zone of north-western Mexico (Figs 1 and 2). The study was undertaken to determine the structural controls on deposition of these units and interpret those controls in light of recent studies of Miocene to Holocene deformation in the region. The deposits are excellently exposed due to recent uplift and deep erosion in the footwall of an active normal fault (Cañon Rojo fault), which occupies a releasing bend in the dextral-normal Laguna Salada fault. Through detailed mapping of sedimentary lithofacies, structures and palaeocurrents, we have reconstructed the Pliocene–Pleistocene history of growth faulting, folding and sedimentation in a complex zone of interaction between extensional and oblique-slip structures near the margin of the basin. This provides a useful example of how extension-related faults and folds control topography and stratigraphic evolution of alluvial fan systems in active transtensional basins, and it helps us to clarify genetic and timing relationships between Pliocene–Pleistocene faulting and basin development in the area. Although the absolute ages of the units examined in this study are not well constrained, the integrative approach used here enables us to better understand the long-term stratigraphic and structural evolution of a complex zone of interaction between oblique-slip and normal faults in an area where deformation and basin evolution have been controlled by transtensional tectonics and detachment faulting from Pliocene time to the present.

TECTONIC SETTING

Laguna Salada is an active transtensional basin in northwest Mexico that has subsided from late Miocene time

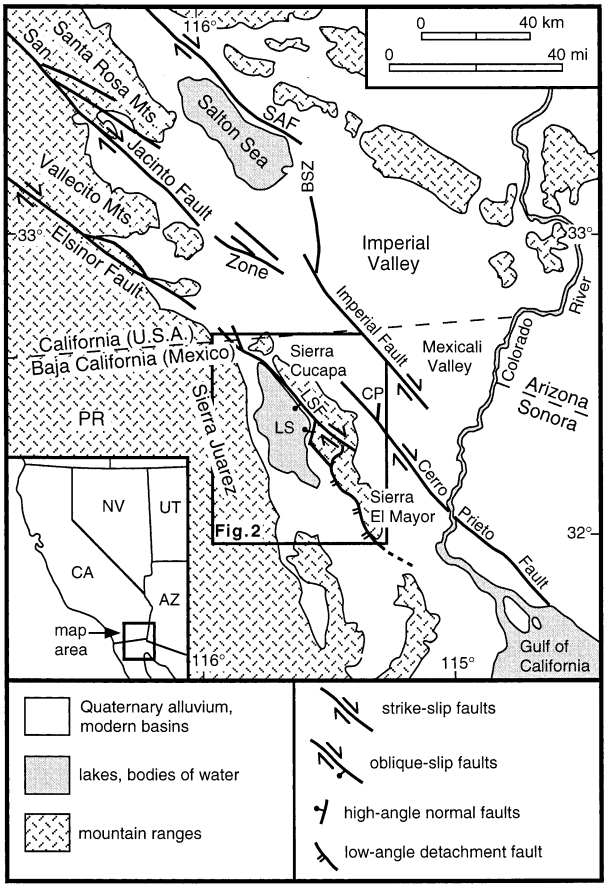

Fig. 1. Simplified tectonic map of NW Mexico and SE California, showing major strike-slip faults and mountain ranges, and location of Fig. 2. BSZ = Brawley seismic zone, CP = Cerro Prieto, LS = Laguna Salada, LSF = Laguna Salada fault. PR = Peninsular Ranges, SAF = San Andreas fault. Modified from Mueller & Rockwell (1995) and Axen *et al.* (1999).

to the present in response to evolution of a large top-to-the-west detachment fault system (Cañada David detachment fault) and the dextral-normal Laguna Salada fault, which together make up the composite NE margin of the basin (Figs 1 and 2; Mueller & Rockwell, 1991, 1995; Gastil & Fenby, 1991; Siem & Gastil, 1994; Axen *et al.*, 1998, 1999; Axen & Fletcher, 1998). Slip on the Cañada David and Monte Blanco detachment faults produced Pliocene to Recent subsidence and sedimentation in the flanking Cerro Colorado, Lopez Mateos and Laguna Salada basins (Fig. 2; Axen & Fletcher, 1998; Axen *et al.*, 1998, 1999). The Laguna Salada fault was initiated sometime in Pliocene time and is seismically active today (Mueller & Rockwell, 1991, 1995; Vázquez-Hernández *et al.*, 1996). The ratio of strike-slip to dip-slip displacement on the Laguna Salada fault has been slightly greater than 1 : 1 over the past $\approx 50\,000$ years, with an average rate of ≈ 2–3 mm yr^{-1} for each component and a recurrence interval of ≈ 1–2 kyr (Mueller & Rockwell, 1995). Slip on the Laguna Salada fault and related high-angle normal faults has been interpreted to entirely post-date movement on the detachment faults (e.g. Gastil & Fenby,

1991; Mueller & Rockwell, 1995), but new work suggests that slip on the southern part of the Cañada David detachment fault has continued through Pleistocene time to the present (Axen *et al.*, 1999), and therefore a portion of the detachment faulting history is concurrent with dextral-normal slip on the Laguna Salada fault. Although local variations are observed in the orientation of fault-kinematic indicators, the overall direction of extension on the composite detachment fault system is east–west, top to the west (Axen & Fletcher, 1998; Axen *et al.*, 1998, 1999). Thus, the Laguna Salada basin and basin-forming faults on its north-east margin have evolved in a complex transtensional tectonic setting that was dominated by strong E–W extension (detachment faults) in late Miocene and Pliocene time, with dextral-oblique slip on the Laguna Salada fault beginning in middle or late Pliocene time and continuing to the present.

The Cañada David detachment fault includes both active strands and an inactive strand (Fig. 2; Axen *et al.*, 1998, 1999). The inactive part (CD-i, Fig. 2) makes up the overall NNE-trending, curved fault contact between crystalline rocks in the Sierra El Mayor and Pliocene–Pleistocene sedimentary rocks exposed in the Cerro Colorado basin to the north-west. Footwall-derived submarine breccias and sandstones in the lower part of the Imperial Formation near the detachment fault indicate that this strand of the fault was active during Pliocene time (Vázquez-Hernández *et al.*, 1996; Vázquez-Hernández, 1996; Axen *et al.*, 1998). It is not well known when slip ceased on the now inactive part of the detachment fault, but the presence of low-angle normal faults that cut Plio-Pleistocene upper-plate sedimentary rocks (Vázquez-Hernández, 1996) suggests that slip may have continued until early or middle Pleistocene time. The active portion of the Cañada David detachment fault (CD-a, Fig. 2) follows the north-eastern margin of the modern Laguna Salada basin from the south end of the Sierra El Mayor to its intersection with the now inactive part of the detachment fault (Fig. 2). This part of the fault system features abundant Quaternary range-front normal fault scarps that recently have been attributed to latest Pleistocene and Holocene slip on the low-angle (29°) detachment fault surface at depth (Axen *et al.*, 1999). Active range-front normal faults (RF, Fig. 2) are present NW of there, between the inactive part of the detachment fault and the south end of the Cañon Rojo fault (Axen *et al.*, 1999). This part of the active fault system is not well studied, but it appears to be a young dextral-normal fault whose slip sense may be similar to that of the Laguna Salada fault (T. Rockwell & G. Axen, 1999, personal communication).

The Laguna Salada fault experienced a widely felt M $\approx$7.1 earthquake in 1892 that produced up to 5 m of surface offset (Mueller & Rockwell, 1991, 1995). The surface rupture broke both the Laguna Salada and the Cañon Rojo faults in the same event, making an $\approx$100° bend at the intersection of the two faults (Figs 2 and 3). This event is representative of active faulting and ongoing patterns of surface uplift, subsidence and sedimentation where the two faults join. In spite of inferred high rates of sediment input from arroyos and cañadas that drain footwall uplifts, the shoreline of Laguna Salada ($\approx$sea level) is located close to the Cañon Rojo fault, probably due to the effects of rapid hangingwall subsidence in a releasing bend geometry (Figs 2 and 3; Mueller & Rockwell, 1995). An exploratory hydrothermal well (ELS-1, Fig. 2) reveals a stratigraphic record of this subsidence: 900 m of silt and fine- to medium-grained sand produced by lacustrine and/or Colorado River flood deposition is underlain by $\approx$800 m of sandstone and conglomerate containing large blocks of granitic basement rock, which is underlain by $\approx$700 m (to the base of the well) of reddish to beige quartzose sandstone equivalent to the Plio-Pleistocene Palm Spring Formation (Garcia-Abdeslem *et al.*, unpublished data, cited in Axen *et al.*, 1998). The 800-m sandstone–conglomerate was inferred by Axen *et al.* (1998) to be roughly equivalent to the redbeds sequence and grey gravel unit of this study. If true, then the overlying 900-m-thick unit of silt and sand would post-date stratigraphic units exposed in the footwall of the Cañon Rojo fault. These correlations are tentative and remain untested.

STRATIGRAPHY

Summary of sequences and age estimates

Stratigraphic relationships in the study area are revealed in the geological map (Fig. 3) and schematic stratigraphic diagram (Fig. 4). Bedrock stratigraphy is divided into three unconformity-bounded sequences (term used informally here): (1) Pliocene Imperial Formation; (2) Pliocene–Pleistocene redbeds sequence; and (3) Pleistocene grey gravel unit (Fig. 4). The Imperial Formation is exposed in the core of a north-plunging anticline (Fig. 3) and consists of greenish marine claystone, mudstone and siltstone with rare thin coquina shell beds. The age of the Imperial Formation in the study area is poorly known. Most observed microfossils in the Imperial Formation are reworked Cretaceous and lower Tertiary forams, nanoplankton and ostracods that were delivered by the ancestral Colorado River, but it also contains benthic forams that indicate a maximum age of early Pliocene (Vázquez-Hernández *et al.*, 1996). The thickness of the Imperial Formation in the study area also is not well constrained. Intact sections up to $\approx$200 m thick have been mapped within fault blocks of the Cerro Colorado basin (Fig. 2; Vázquez-Hernández *et al.*, 1996), but the whole formation probably is considerably thicker than that and may be 500–1000 m thick or more (Axen *et al.*, 1998). The contact with the overlying Palm Spring Formation is poorly exposed, but based on its sharp nature in the study area and recent work nearby to the south (Vázquez-Hernández *et al.*, 1996; Vázquez-Hernández, 1996), the contact is interpreted as an unconformity.

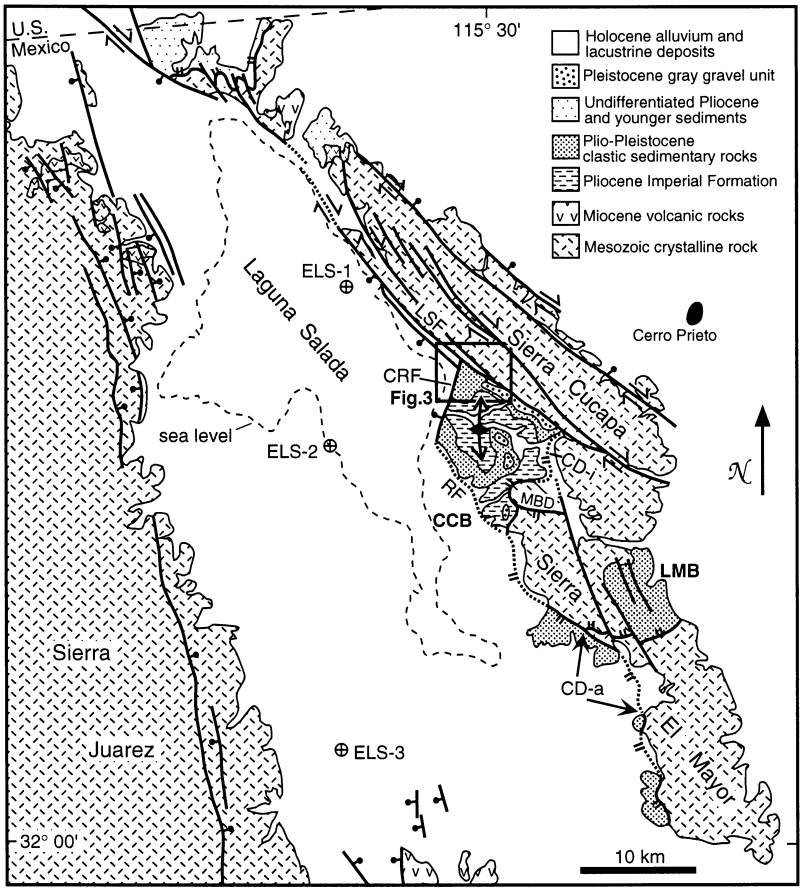

Fig. 2. Simplified geological map of the Laguna Salada area showing major faults, sedimentary sequences, modern Laguna Salada basin, and location of Fig. 3. CCB = Cerro Colorado basin, CD-a = active portion of Cañada David detachment, CD-i = inactive portion of Cañada David detachment, CRF = Cañon Rojo fault, LSF = Laguna Salada fault, MBD = Monte Blanco detachment, RF = range-front fault scarps along active continuation of Cañada David detachment fault. Double-headed arrow south-east of Cañon Rojo fault represents large anticline in upper plate of inactive portion of Cañada David detachment fault. Modified from Axen *et al.* (1998, 1999); fault symbols as in Fig. 1. See Fig. 1 for location.

The redbeds sequence is a thick package of laterally variable and interfingering lithofacies that include: boulder breccia and conglomerate, sandy conglomerate, conglomeratic sandstone (all having no formal formation name), and sandstone, siltstone and claystone of the Palm Spring Formation (Fig. 4). These units display rapid lateral fining away from the Laguna Salada fault. The thickness of the redbeds sequence is estimated from map relationships and cross-sections (Figs 3 and 7) to be ≈900–1000 m. The age of the redbeds sequence is poorly constrained. Based on its position above the Pliocene Imperial Formation and below the grey gravel unit, and by comparison with similar sections in the Salton Trough to the north (Woodard, 1974; Dibblee, 1984; Winker, 1987; Winker & Kidwell, 1996), it is inferred to be late Pliocene to early Pleistocene in age. Breccia, conglomerate and conglomeratic sandstone facies are composed of tonalitic detritus shed from the Sierra Cucapa to the north-east, indicating that the Laguna Salada fault was active during redbeds deposition. By contrast, sand and silt in the Palm Spring Formation consist of well-rounded quartz derived from the ancestral Colorado River (Vázquez-Hernández, 1996; Winker & Kidwell, 1996). The redbeds sequence is named for the distinctive deep to pale red colour of hematite-cemented breccia, conglomerate and conglomeratic sandstone units. The Palm Spring Formation is not red, but it is included in the redbeds sequence because of its lateral interfingering and interbedding with locally derived coarse-grained red units (Fig. 4).

The grey gravel unit overlies the redbeds sequence along an angular unconformity. Based on stratigraphic position above the redbeds section, uncemented nature and great thickness, it is inferred to be early or middle Pleistocene in age. This estimate is highly uncertain. Map relations, topography and extrapolation of gentle bedding dips (Figs 3 and 7) indicate that it is ≈600 m thick. The youngest units in the study area consist of relatively thin, unconsolidated Quaternary deposits that are preserved in a succession of raised terraces cut into older bedrock stratigraphy, and modern alluvium accumulating in present-day stream channels and alluvial fans (Fig. 4; Mueller & Rockwell, 1991, 1995).

Redbeds sequence

Palm Spring Formation

The Palm Spring Formation in the study area consists of weakly to moderately cemented, interbedded fine- to very fine-grained sandstone, siltstone, mudstone and claystone in subequal amounts. Sandstone in the Palm Spring Formation is thin- to medium-bedded (3–30 cm), displaying both horizontal bedding and cross-bedding, and it typically occurs in sharp-based fining-up intervals

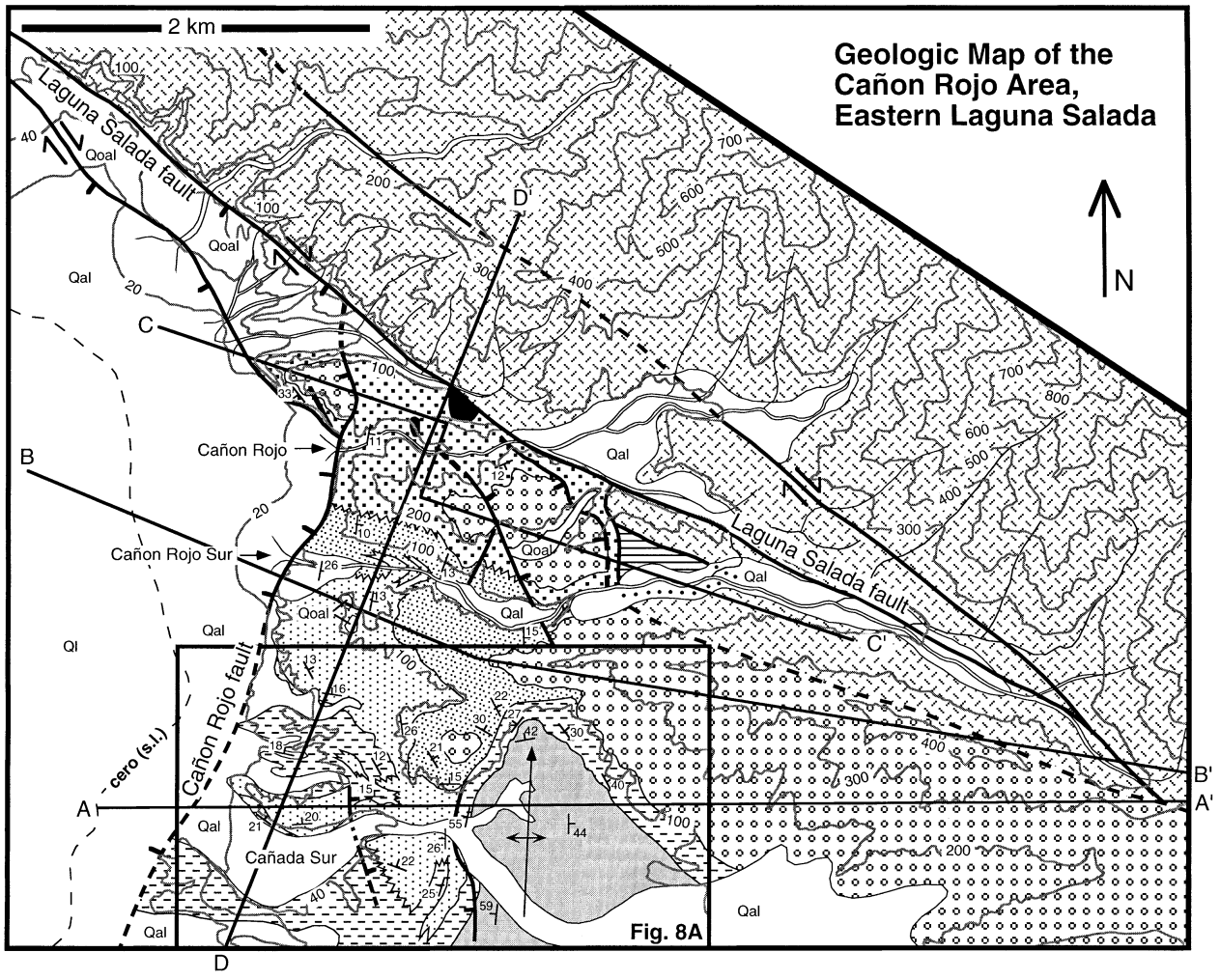

Fig. 3. Geological map of the Cañon Rojo study area. See Fig. 2 for location.

1–3 m thick that display both planar and channellized bases. Sandstone and siltstone intervals alternate with beds of reddish to purple mudstone and claystone up to ≈1 m thick that commonly display diffuse to dense internal mottling. Thin tabular beds of nodular calcite are also present. Detrital fine-grained sand and silt is composed of well-rounded, well-sorted quartz.

The above observations indicate that the Palm Spring Formation accumulated in a low-energy nonmarine depositional system in which traction sedimentation of fine-grained sand alternated with suspension settling of clay and silt. Nodular calcite and mottled red claystone represent palaeosols. The above conditions are typical of low-energy fluvial systems in which suspension settling in broad overbank and flood plain settings alternates with soil development and input of sand by stream floods and

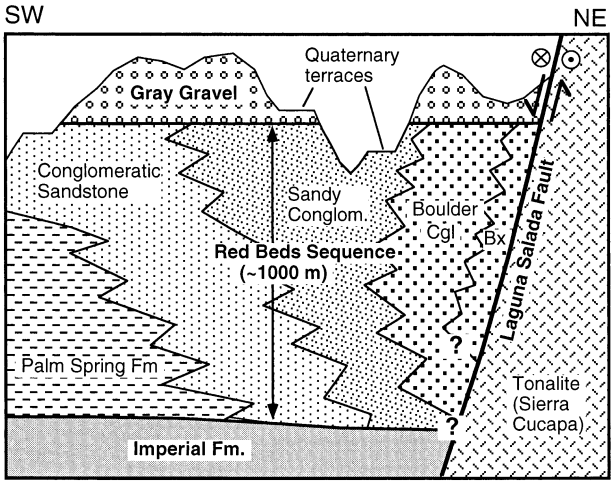

Fig. 4. Schematic diagram of stratigraphic relationships and nomenclature for Pliocene–Pleistocene sedimentary rocks in the Cañon Rojo area (Fig. 3). Patterns as in Fig. 3. Bx = breccia, Cgl = conglomerate.

formation of crevasse splays (e.g. Reineck & Singh, 1980; Collinson, 1986). These deposits accumulated in the lower reaches of the ancestral Colorado River and delta system, with fine-grained detrital quartz derived from older, Mesozoic sedimentary units in the Colorado Plateau (e.g. Winker, 1987; Winker & Kidwell, 1996).

Conglomeratic sandstone

Conglomeratic sandstone consists of moderately to poorly sorted, thin- to medium-bedded, fine- to coarse-grained sandstone and pebbly sandstone with thin discontinuous lenses of clast-supported pebble and pebble-cobble conglomerate (Fig. 5A). Bedding is characterized by uneven horizontal stratification with minor low-angle cross-stratification and rare shallow channels. Exposed sections typically display no vertical variations in overall grain size or bedding style and thickness. Sand and gravel is composed entirely of tonalite derived from the Sierra Cucapa.

The abundance of planar stratification in poorly sorted pebbly sandstone, combined with a lack of cross-bedding and channel forms, indicates that conglomeratic sandstone was deposited by sheet floods in the lower, sand-rich part of one or more low-gradient alluvial fans. Rapid traction sedimentation by shallow upper plane bed flood flows explains the presence of poor sorting, clast imbrication, crude discontinuous horizontal stratification, and overall lack of channels and cross-bedding. Sheet flooding commonly occurs in alluvial fan systems when sediment-charged flash floods exit at the mouth of an incised canyon and flow across the unconfined fan surface, rapidly depositing the bedload in diffuse sheets (Bull, 1972; Rust & Koster, 1984; Wells & Harvey, 1987; Blair & McPherson, 1994).

Sandy conglomerate

Sandy conglomerate has two variants that are distinguished on the degree of sorting and presence or lack of discrete sandstone interbeds. The first variant consists of tabular to broadly lenticular, medium to thick beds (typically $\approx$30–100 cm) of moderately sorted, clast-supported pebble–cobble conglomerate. These are interbedded with similar-thickness or slightly thinner intervals of horizontally stratified sandstone, pebbly sandstone and sand-rich granule conglomerate (Fig. 5B). Broad, shallow ($<$1 m) scoured channel geometries are sometimes observed, resulting in broad pinch-out and lenticular geometry of sand-rich units. The second variant consists mainly of poorly sorted, weakly bedded, clast-supported, sandy pebble–cobble conglomerate with clasts ranging up to small boulder size ($\approx$30 cm diameter) (Fig. 5C). Thin discontinuous lenses of horizontally stratified pebbly sandstone are present in the second variant, and conglomerate tends to be internally structureless. Clast imbrication is common in conglomerate beds of both variants.

Based on abundance of crude planar stratification, clast imbrication and overall moderate to poor sorting, we interpret sandy conglomerate to be the deposits of gravel-bearing sheet floods that accumulated in the proximal parts of low-gradient, sheet-flood dominated alluvial fans (Bull, 1972; Rust & Koster, 1984; Wells & Harvey, 1987; Blair & McPherson, 1994). Discrete interbedding of conglomerate and pebbly sandstone in the first variant appears to represent sheet-flood couplets produced by flow surges related to migration and washout of antidune bedforms during flood events (e.g. Blair, 1987; Blair & McPherson, 1994). Discontinuous sandstone lenses in the second variant probably record sand deposition during similar flow surges, with most of the sand being removed by subsequent erosion and deposition by gravel-rich flows. Variations in relative abundance of gravel and sand may reflect more proximal and more distal positions on the fan surface, relative to either the fan head or individual sheet-flood lobes.

Boulder conglomerate and breccia

Boulder conglomerate and breccia are grouped together in the same map unit (Fig. 3) due to similarities in areal distribution (proximal to Laguna Salada fault), poor sorting and coarse clast size. Within this unit, breccia facies is found only within $\approx$300–400 m of the Laguna Salada fault. Boulder conglomerate consists of poorly sorted, thick-bedded massive conglomerate with moderately to well-rounded clasts of tonalite ranging from pebble to boulder grade (Fig. 6A). Larger, outsized clasts are 1–2 m in diameter. Boulder conglomerate typically displays clast-supported texture and contains pockets of imbrication in cobble and boulder-size clasts. Weakly developed bedding units are $\approx$1–5 m thick and are recognized by slight clast-size and colour variations between units. Boulder breccia has the same range of clast sizes as boulder conglomerate, but hematite-cemented matrix is more abundant, bedding is absent and clasts are dominantly angular to subangular (Fig. 6B).

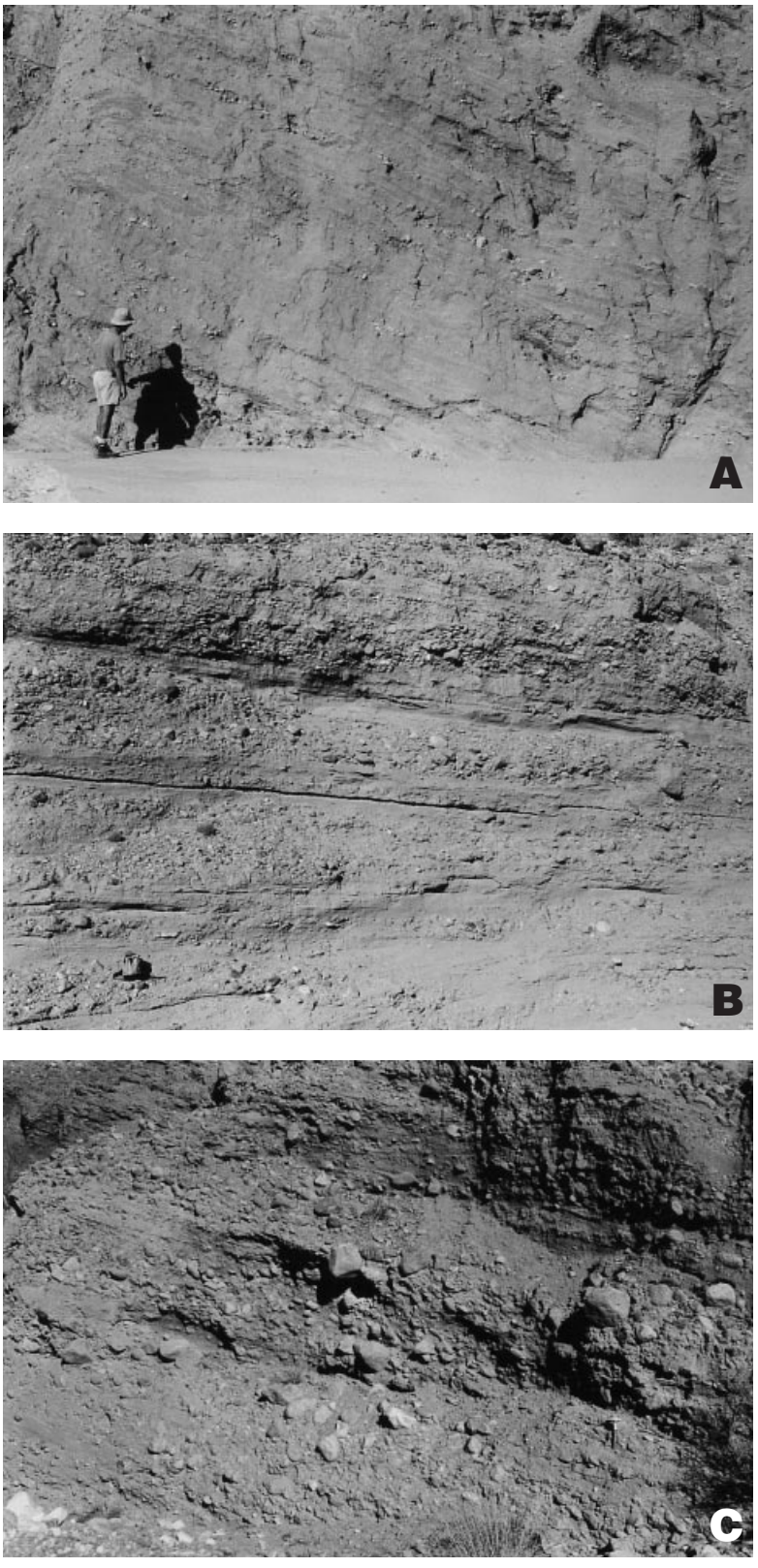

Fig. 5. Outcrop photographs of sedimentary lithofacies in redbeds sequence. A. Outcrop of conglomeratic sandstone facies, interpreted as sheet-flood deposits. B. First variant of sandy conglomerate facies (medial to proximal sheet-flood deposits), showing tabular interbedding of conglomerate and sandstone. Day pack is $\approx$45 cm long. C. Second variant of sandy conglomerate facies (proximal sheet-flood and channel deposits). Hammer (lower right) is 32.5 cm long.

Several large, heavily fractured and brecciated blocks of tonalite, 100–200 m in diameter, are encased within massive, unbedded boulder breccia close to the Laguna Salada fault (Fig. 3).

Boulder conglomerate and breccia are interpreted as proximal fault-scarp facies of the Laguna Salada fault. The combination of poor sorting, thick bedding, partial clast-supported fabric, local clast imbrication and lack of internal stratification indicates that boulder conglomerate was deposited by noncohesive boulder-rich debris flows (e.g. Rust & Koster, 1984; Blair & McPherson, 1994). By contrast, the matrix-supported fabric and lack of

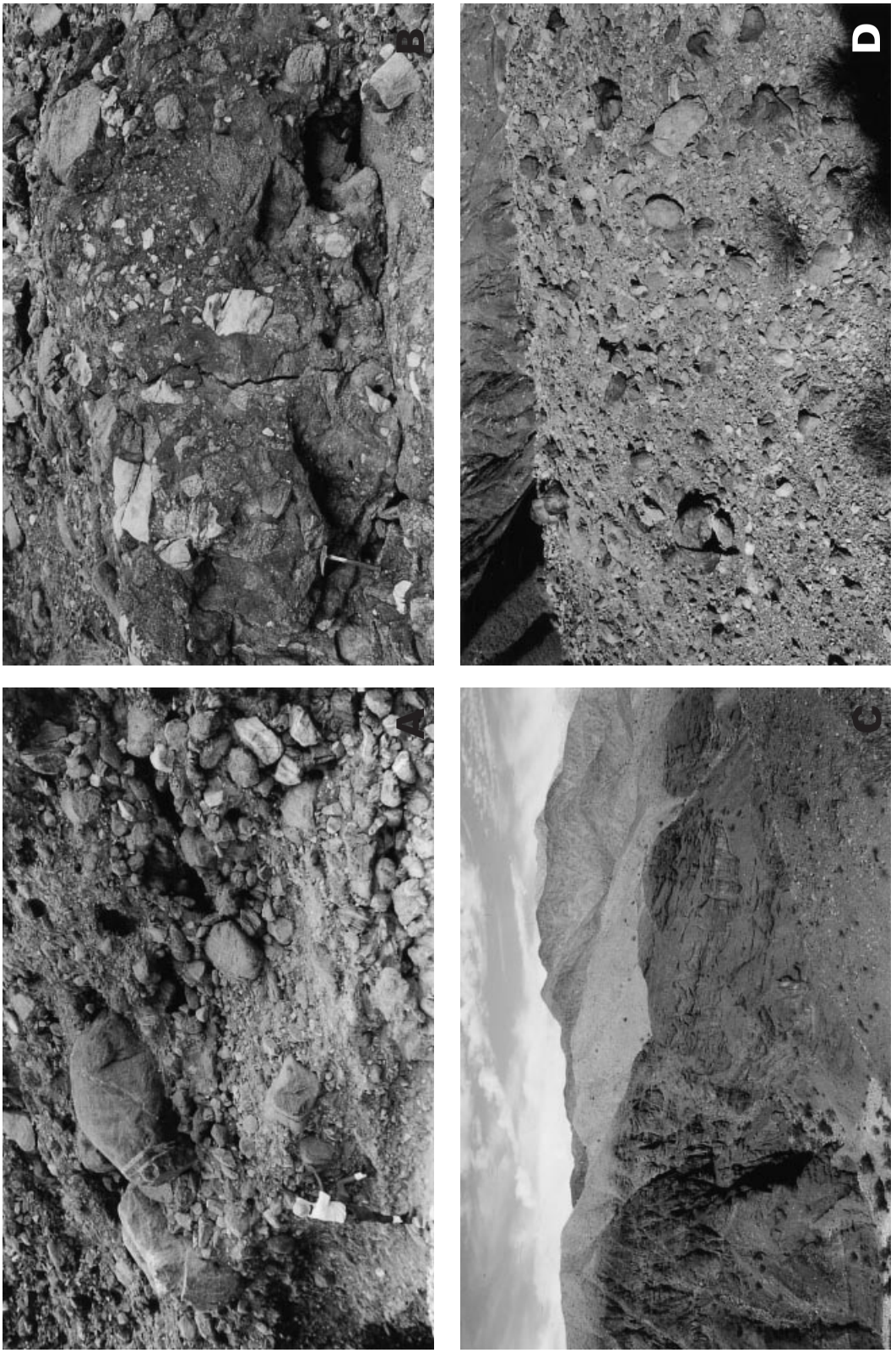

Fig. 6. Outcrop photographs of redbeds and grey gravel. A. Boulder conglomerate facies, showing poor sorting, massive texture and moderate rounding of clasts. B. Boulder breccia facies, showing unsorted texture and abundance of angular clasts. C. View looking north-east across Cañon Rojo Sur (Fig. 3) at deeply dissected redbeds sequence (boulder conglomerate) and overlying grey gravel (light coloured unit with smooth weathering surface). Unconformity at base of the grey gravel unit dips 8° to the ENE; darker hills in background are tonalite in the Sierra Cucapá. Thickness of conglomerate beneath grey gravel on left side of photograph is about 140 m. D. Outcrop of grey gravel unit showing abundance of boulder tonalite clasts and overall massive, clast-supported texture. Large white clast in right centre is ≈1.2 m long.

imbrication and internal organization in the breccia facies indicate that it accumulated by deposition from cohesive debris flows and landslides. Large blocks of tonalite were emplaced by rock slides and small rock avalanches that may have been triggered by earthquake shaking. The predominance of debris-flow and rock-avalanche deposits, lack of sheet-flood facies and palaeocurrents consistently directed toward the south-west (see below) provide evidence that this unit accumulated in short, steep, debris-flow-dominated alluvial fans shed from the footwall of the Laguna Salada fault.

Grey gravel unit

This unit is the youngest stratigraphic sequence recognized in the study. It overlies the redbeds sequence along an angular erosional unconformity that is marked by an abrupt change from deep red, hematite-cemented sedimentary rocks below to pale grey, unconsolidated slope-forming gravels above (Fig. 6C). The unconformity at the base of the grey gravel unit shows variable discordance with underlying units in the map area. In the southern part of the area it is an angular unconformity that truncates steeply dipping limbs of the anticline (Figs 7A and 9), and in the north it is nearly concordant with underlying units (Fig. 7C,D). In the northern part of the mapped area, the measured dip on the basal contact is 8° to the ESE (Fig. 7C). When viewed in a NNE-trending cross-section parallel to the Cañon Rojo fault, the contact is a planar surface that dips consistently ≈3° to the NNE, toward the Laguna Salada fault (Fig. 7D).

Because of its unconsolidated nature and lack of fresh stream cuts, the internal stratigraphy, sedimentology and bedding features of this unit were seldom directly observed. But several exposures show that it consists of poorly sorted, clast-supported, weakly bedded gravel with moderately to well-rounded clasts of tonalite ranging from pebble to boulder size (Fig. 6D). Pale grey slopes display a uniform concentration of tonalite boulders averaging 40–100 cm in diameter, indicating an abundance of boulder-rich deposits and lack of finer-grained conglomerate or sandstone interbeds. The sedimentology of this unit thus is similar to that of the boulder conglomerate facies in the redbeds sequence, and is similarly interpreted to record deposition by noncohesive boulder-rich debris flows derived from the footwall of the Laguna Salada fault.

STRUCTURE

Growth anticline and related folds

The southern part of the study area contains a large growth anticline, cored by the Imperial Formation, in the footwall of the Cañon Rojo fault (Figs 3, 7A,B and 8). The anticline has an amplitude of ≈600 m and is slightly asymmetric, with bedding dips of ≈55° on the west limb and 30–40° on the east limb. The axes of this and related folds to the east trend consistently north to NNE, parallel to the strike of associated normal faults and perpendicular to the direction of extension. They are thus classified as 'longitudinal folds' (Schlische, 1995; Janecke *et al.*, 1998), and their origin and kinematic relation to regional extension are explored below (see Discussion). The dashed lines above the angular unconformity (Figs 7A and 8B) represent the extrapolated trace of the anticlinal hinge as it probably looked prior to erosion and deposition of the grey gravel unit.

Growth folding relationships are revealed by detailed mapping and cross-section geometries (Fig. 8). The basal unit of the Palm Spring Formation maintains a constant thickness across the anticline and flanking broad syncline to the west, and thus represents the youngest pregrowth unit of this structure. Above that we see pronounced thickening of strata westward away from the west limb of the anticline, systematic eastward convergence of bedding surfaces with eastward pinch-out of strata onto the west limb of the anticline, and fanning of dips in the area of lateral interfingering between conglomeratic sandstone and Palm Spring Formation (Fig. 8B). These relationships provide evidence for progressive syndepositional tilting of strata as a result of limb rotation by fold growth (e.g. Hardy & Poblet, 1994; Ford *et al.*, 1997). The thickest recognized section of growth strata consists of ≈560 m of Palm Spring Formation that includes two tabular units of conglomeratic sandstone (Fig. 8B). The youngest synfolding deposits are difficult to identify, but it appears from palaeocurrent data (next section) that folding slowed during deposition of a ≈200-m-thick conglomerate unit located at the north-west corner of the anticline (Fig. 8A). The map pattern shows that this conglomerate laps onto the west limb of the anticline along a buttress unconformity. Stratigraphic onlap of this nature could have been produced either during or after fold growth, but the palaeocurrent data suggest that folding continued during deposition of the lower half of this conglomerate unit and probably ended by the time of deposition of the upper part. From the above relationships, we infer that growth of the anticline and associated syncline to the west began shortly after the beginning of Palm Spring deposition and continued during most of redbeds deposition.

Cañon Rojo fault

The Cañon Rojo fault is a large active structure that cuts all stratigraphic units in the study area. Total offset on this fault is estimated by considering the geometries and stratal thicknesses shown in cross-section B–B′ (Fig. 7B). The grey gravel unit is ≈600 m thick based on its gentle eastward dip and basic constraints from topography (Fig. 7B). Because cross-section B–B′ is close to the Laguna Salada fault where subsidence and sediment accumulation are known to be high, we assign the same thickness (600 m) to the grey gravel unit in the hangingwall of the Cañon Rojo fault. We conservatively assign a thickness of ≈200 m to lacustrine sediment above the

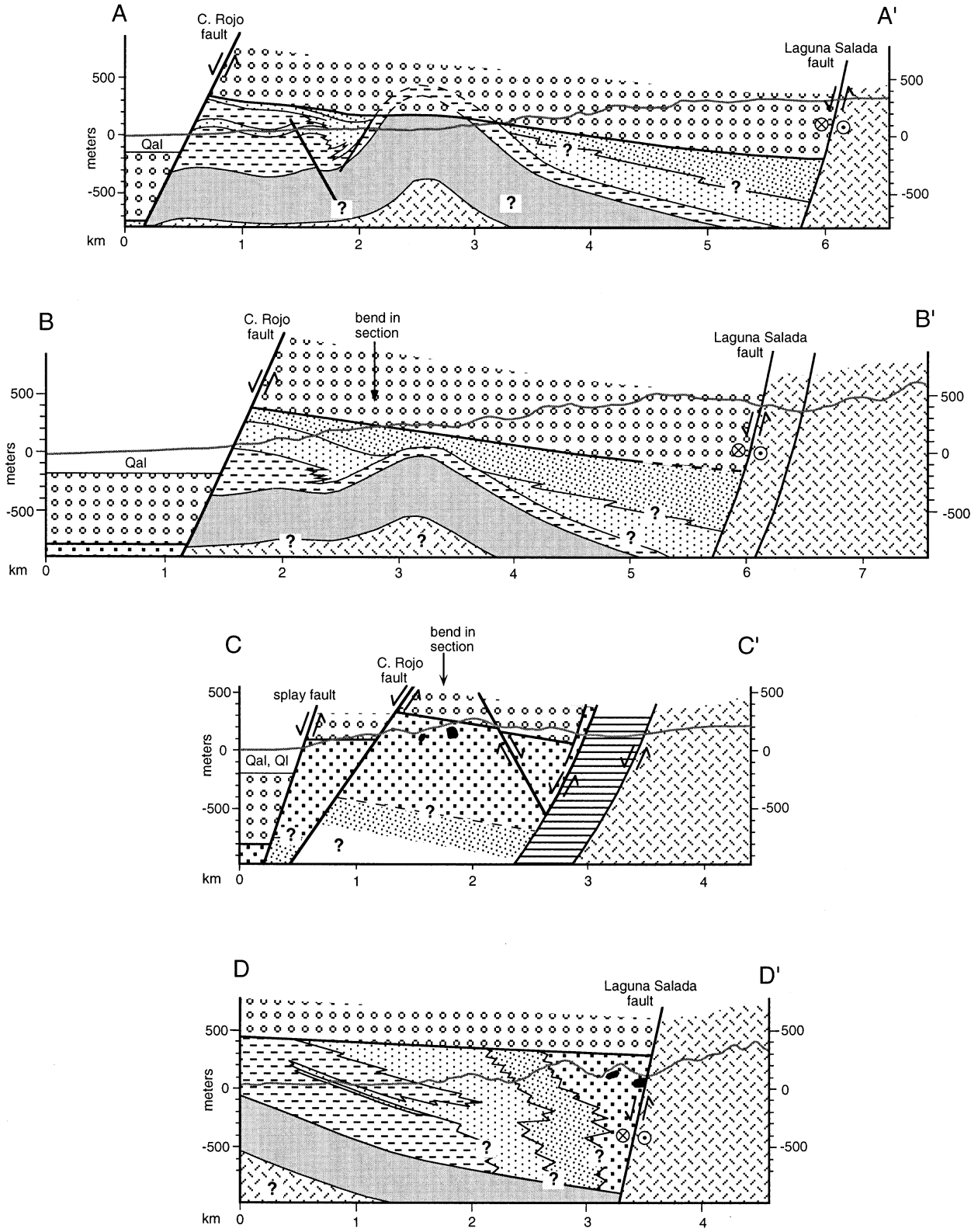

Fig. 7. Four cross-sections in the Cañon Rojo area showing key structures and stratigraphic relationships. Location of sections and patterns are shown in Fig. 3. Structural relationships at depth are speculative and inferred from map relations.

grey gravel unit, although this is probably an underestimate. From these thicknesses and cross-section relationships (Fig. 7B) we derive a minimum total offset of 1300 m on the Cañon Rojo fault.

The long-term rate of slip on the active Cañon Rojo fault is estimated from the thickness and likely age of offset Pleistocene units. Assuming an early to middle Pleistocene age for the grey gravel unit, the top of it is

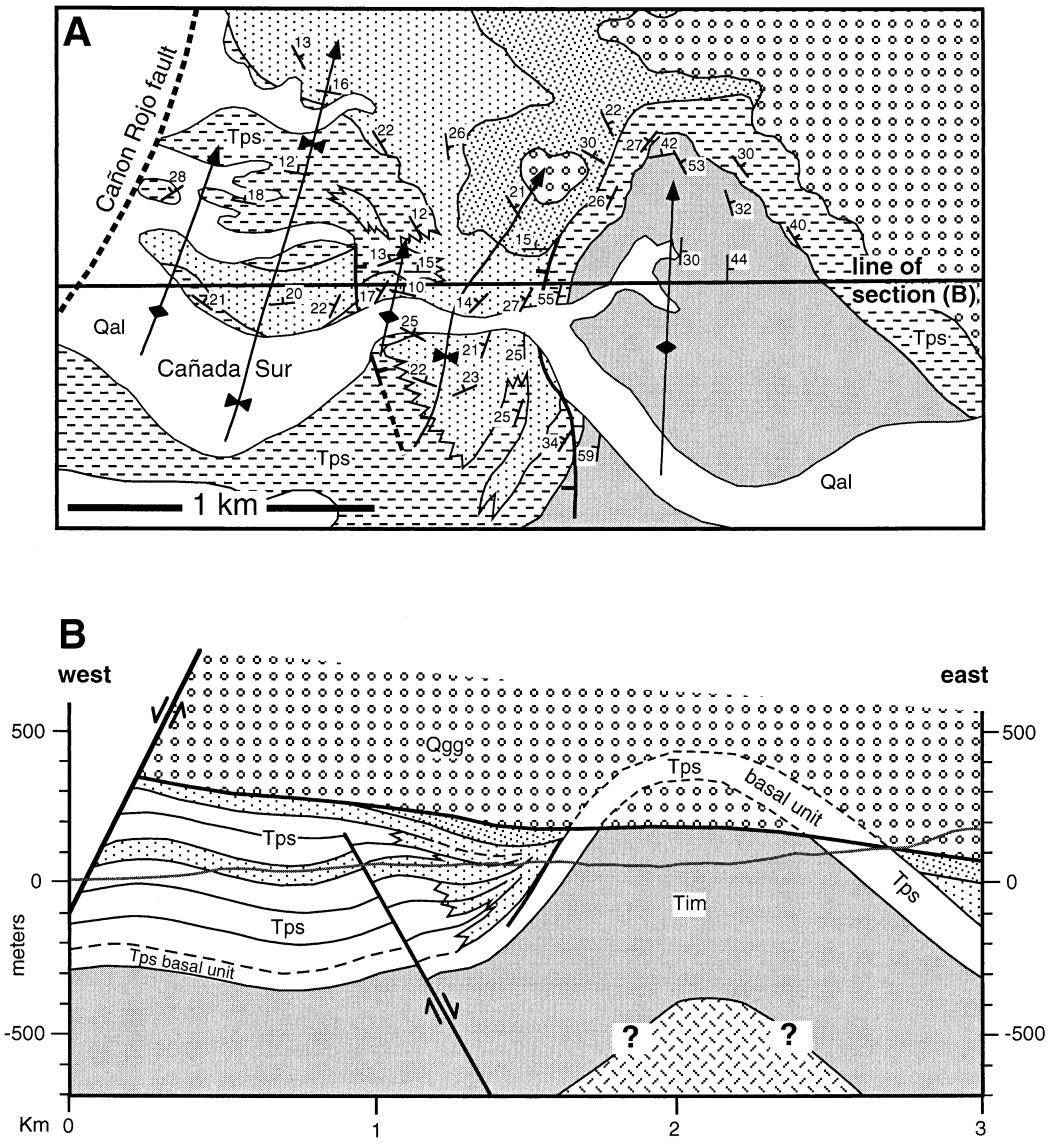

Fig. 8. Detailed geological map (A) and cross-section (B) of growth anticline and redbeds stratigraphy in southern part of study area. Patterns are same as in Fig. 3. See Fig. 3 for location.

tentatively bracketed between ≈1.0 and 0.5 Ma. Offset of 1300 m over a period of 0.5–1.0 Myr yields a time-averaged slip rate of 1.3–2.6 km Myr^{-1} (1.3–2.6 mm yr^{-1}). This appears to be a minimum estimate because the top of the grey gravel unit may be younger than is assumed here, it may originally have been more than 600 m thick and the thickness of lacustrine sediment overlying grey gravel in the hangingwall is probably greater than 200 m (Fig. 7B). If we instead set hangingwall subsidence equal to footwall uplift, we predict the top of the grey gravel unit to be ≈900 m below the lake surface, which is reasonable based on a tentative comparison with well ELS-1 (Fig. 2). In this case, the total offset would be ≈2 km and the time-averaged slip rate is 2–4 km Myr^{-1} (2–4 mm yr^{-1}). This is similar to the dip-slip component of oblique slip on the Laguna Salada fault (≈2–3 mm yr^{-1}) that was estimated by Mueller & Rockwell (1995) based on study of faulted upper Pleistocene to Holocene alluvial fan deposits.

Laguna Salada fault

Gently (≈15–20°) NNE-dipping redbeds and NNE-plunging folds in the footwall of the Cañon Rojo fault allow us to project a thick section of lithologically diverse stratigraphy of the redbeds sequence toward the Laguna Salada fault (cross-section D–D′; Fig. 7D). Nearly 1000 m of proximal boulder breccia and conglomerate derived from the footwall of the Laguna Salada fault pass laterally southward into sandy conglomerate, conglomeratic sandstone and Palm Spring Formation. The thick accumulation of tonalitic gravel and sand provide evidence that the Laguna Salada fault was active and created substantial footwall uplift and hangingwall subsidence

during deposition of the redbeds sequence. Intersection of cross-sections shows that the unconformity at the base of the grey gravel unit is a planar surface that dips consistently $\approx 3^\circ$ to the NNE toward the Laguna Salada fault (Fig. 7D). The above geometries record a long history of gradual NNE-ward tilting that was produced by the dip-slip (normal) component of displacement on the Laguna Salada fault. Total slip on the Laguna Salada fault decreases considerably south-east of the Cañon Rojo fault because a large amount of slip is transferred to the Cañon Rojo fault (Fig. 3).

Other faults

In the northern part of the mapped area, proximal deposits of boulder conglomerate, breccia and grey gravel are cut by several high-angle normal faults that appear to splay or merge with the Laguna Salada fault (Figs 3 and 7C). The easternmost fault in cross-section C–C′ is a down-on-the-west normal fault that juxtaposes proximal boulder breccia on the west against a fault block of Palaeozoic metamorphic rock, which is faulted against footwall tonalite. Based on abundance of fault-scarp breccia facies and WNW-directed palaeocurrents in boulder conglomerate close to this fault, we infer that it was active during deposition of the redbeds sequence.

PALAEOCURRENTS

Boulder conglomerate, sandy conglomerate and conglomeratic sandstone facies in the redbeds sequence display abundant clast imbrication that permit detailed palaeocurrent analysis. The data are grouped according to geographical location and lithofacies (Fig. 9). Most palaeocurrents collected from boulder conglomerate record consistent transport toward the SW (Fig. 9A), with one small area showing WNW-directed transport (Fig. 9B). This appears to be controlled by palaeogeographical position rather than a change of transport direction through time, because most of the data were collected from approximately age-equivalent strata. Figure 9(C) reveals consistent palaeotransport toward the WNW, perpendicular to the Cañon Rojo fault and the axis of the growth anticline. Finally, an up-section change is seen in a ≈ 80-m-thick section of sandy conglomerate preserved in the growth syncline ≈ 100 m west of where these strata onlap onto the west limb of the growth anticline (Fig. 3). Palaeocurrents are directed toward the SSW in the lower part of the section (Fig. 9D) and toward the NW in the upper part of the section (Fig. 9E). This change in palaeocurrent direction occurs about half way up the 80-m section with virtually no stratigraphic overlap between the two orientations of palaeocurrent data.

Palaeocurrents in the study area can be interpreted in terms of palaeogeography, sediment-dispersal systems, and deposition on alluvial fans. SW-directed palaeocurrents in most localities of boulder conglomerate (Fig. 9A) record deposition in short, steep alluvial fans that were shed directly from the adjacent footwall of the Laguna Salada fault to the NE. In one exception to this pattern, WNW-directed palaeocurrents at the easternmost locality of boulder conglomerate (Fig. 9B) record transport and deposition in coarse, boulder-rich alluvial fans derived directly from the footwall of the unnamed normal fault just to the east. Further to the south, abundant WNW-directed palaeocurrents in sandy conglomerate and sandstone (Fig. 9C) record deposition in low-gradient, coalescing alluvial fans that were ultimately derived from tonalite bedrock on the NE side of the Laguna Salada fault. Streams that fed these low-gradient fans apparently flowed to the WNW across and around the large anticline as it was growing, in a pattern similar to that seen in the large cañadas that traverse the footwall of the Cañon Rojo fault today (Fig. 3).

INTERPRETATION AND DISCUSSION

Basin reconstruction

Our reconstruction of the Pliocene–Pleistocene depositional basin and bounding structures is based on data presented above, consideration of relationships with neighbouring active and inactive faults, and comparison with other studies of similar basins and related structures. Deposition of the redbeds sequence is interpreted to have taken place in a supradetachment basin (cf. Friedmann & Burbank, 1995) in the upper plate of the Cañada David detachment fault (Fig. 10). The thick stratigraphic package (>1000 m) accumulated in a rapidly subsiding depocentre that formed by the combination of synclinal downwarping on the west flank of the growth anticline to the east and dextral-normal slip on the Laguna Salada fault to the north. Syndepositional growth of the anticline and syncline apparently resulted from slip of the upper plate over a large bend in the detachment fault surface at depth (Fig. 10; see additional discussion below).

Two kinds of alluvial fans were produced during deposition of the redbeds sequence: (1) short, steep, debris-flow-dominated fans that were sourced in small footwall drainages and accumulated on active scarps of the Laguna Salada fault; and (2) large, low-gradient, sheet-flood-dominated fans fed by large cañadas that crossed from the footwall to the hangingwall of the Laguna Salada fault and traversed across the growth anticline (Fig. 10). This model is based on palaeocurrent data and distribution of sedimentary lithofacies (Fig. 9), and it employs a useful distinction between debris-flow- and sheet-flood-dominated alluvial fans (Blair & McPherson, 1994). Boulder conglomerate and breccia (representing debris flows and small rock avalanches) are restricted to areas close to the Laguna Salada fault, and they record a short distance of transport to the SW away from the footwall. By contrast, sandy conglomerate and conglomeratic sandstone (sheet-flood facies) are located further from their footwall source and record transport to the WNW across

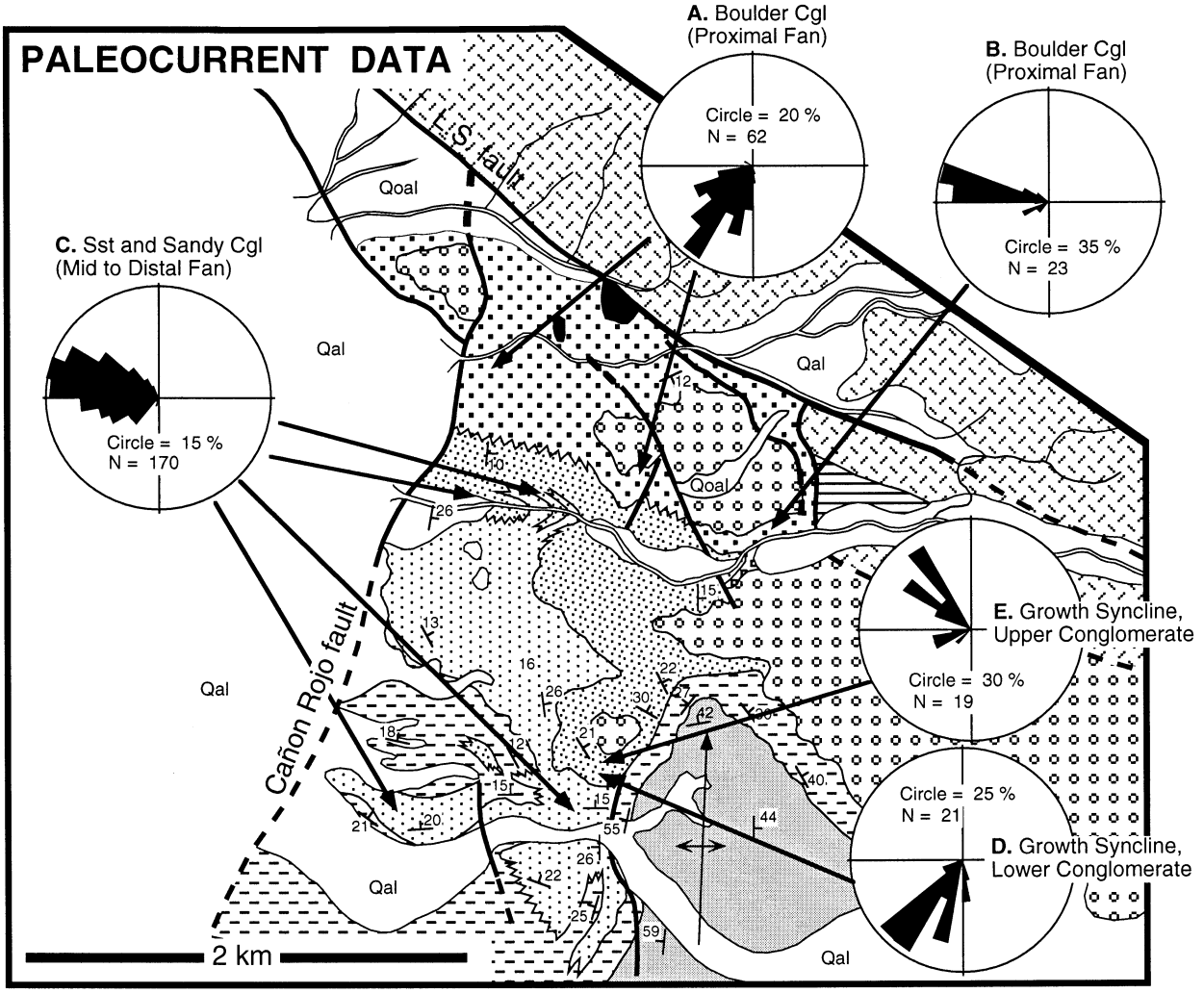

Fig. 9. Rose diagrams of palaeocurrent data collected from imbricated clasts in conglometrate of the redbeds sequence. Patterns are same as in Fig. 3.

the supradetachment basin (Fig. 10). Lateral interfingering of debris-flow and sheet-flood facies represents the merging of these two systems where short steep fault-scarp fans impinged on lower-gradient alluvial fans.

The abrupt up-section change of palaeocurrents seen in sandy conglomerate of the growth syncline (Fig. 9D,E) is interpreted to record a change in the balance between rate of fold growth and rate of sediment accumulation (Fig. 11). During deposition of conglomerate in the lower half of this section, the rate of fold growth was sufficiently fast relative to sediment aggradation that the anticline formed a NNE-trending ridge and the syncline created a subtle topographic trough, resulting in transport of sediment toward the SSW along the axis of the syncline (Fig. 11A). Later, due to either a decrease in the rate of fold growth or an increase in the rate of sediment aggradation, sediments filled the structural relief between the syncline trough and anticline crest, breaching the crest of the growth anticline and establishing a new, NW-flowing dispersal system across the buried anticline (Fig. 11B). We attribute this upsection change to slowing of fold growth. Erosion in the second phase may also explain the planar geometry seen in map pattern along the contact between the pregrowth lower unit of the Palm Spring Formation and sandy conglomerate that unconformably overlies it in the hinge of the anticline (Figs 3 and 8A). These relationships among folding, sediment transport and palaeocurrent evolution are similar to those recently documented for fold growth in contractional settings (Burbank *et al.*, 1996).

Origin of extension-related folds

Extension-related folds may be orientated parallel (longitudinal), perpendicular (transverse) or oblique to the strike of related normal faults, and they can form by a variety of processes involved in the growth of high- and low-angle normal faults (Groshong, 1989; Withjack *et al.*, 1990; Schlische, 1995; Xiao & Suppe *et al.*, 1997; Janecke *et al.*, 1998). Onlapping and convergence of bedding surfaces and fanning-dip geometries (Fig. 8B) indicate that the large anticline and related longitudinal folds in the study area grew during deposition of the redbeds sequence, prior to deposition of the grey gravel unit.

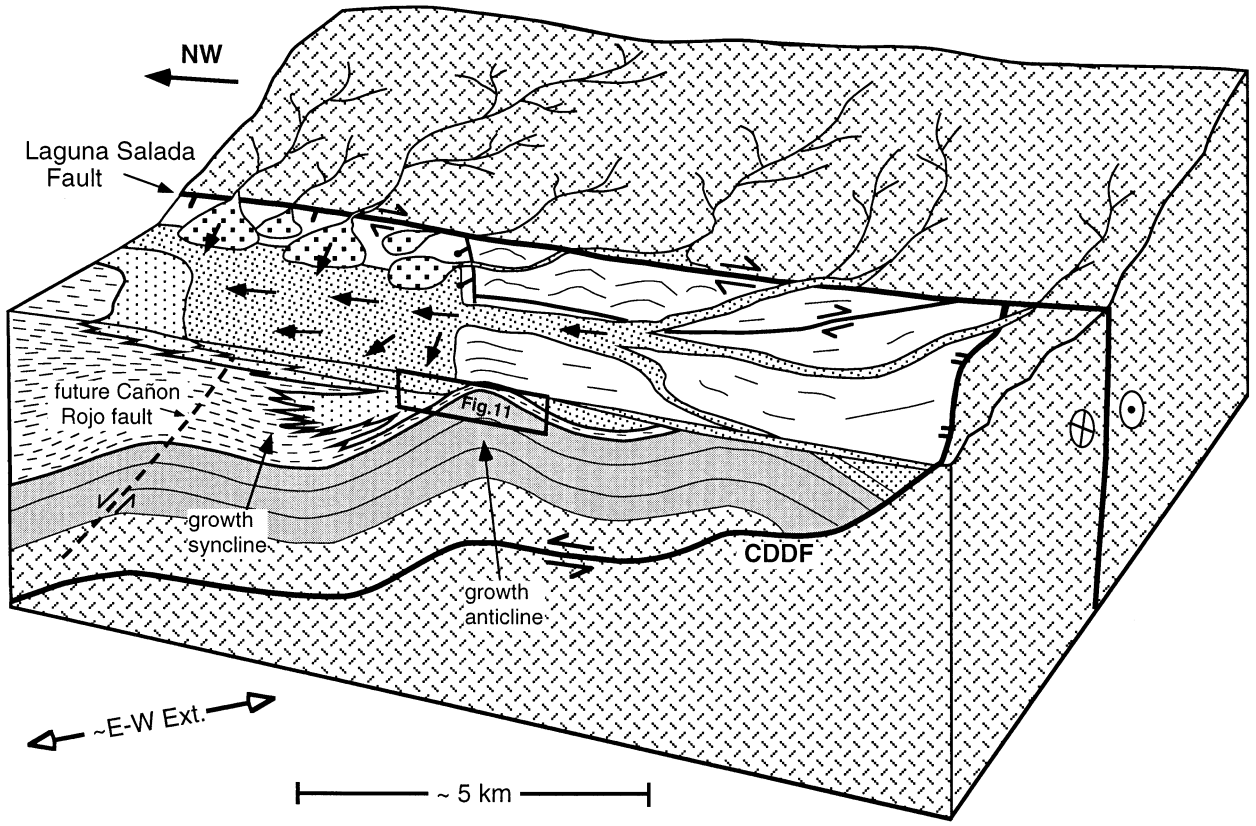

Fig. 10. Schematic diagram showing conceptual model for deposition of redbeds sequence in transtensional supradetachment basin, with growth anticline produced by slip over a large bend in the Cañada David detachment fault (CDDF). See text for discussion.

These geometries are similar to those seen in recent studies of syndepositional folding in both extensional and contractional settings (Hardy & Poblet, 1994; Burbank *et al*., 1996; Ford *et al*., 1997; Gawthorpe *et al*., 1997; Gupta *et al*., 1999). The origin of longitudinal folds in extensional settings can be difficult to determine in the absence of subsurface data, and their interpretation therefore often relies on map relationships with neighbouring structural and tectonic elements. We considered two likely interpretations for the extensional growth anticline and associated smaller folds in the study area: (1) fault-propagation folds that grew above the migrating tips of buried normal faults (e.g. Withjack *et al*., 1990), with domino-style block tilting; or (2) fault-bend folds formed by deformation of the hangingwall as it slipped over one or more ramp-flat bends in the underlying detachment fault (e.g. Tankard *et al*., 1989; McClay & Scott, 1991; Janecke *et al*., 1998). Many of the field observations are consistent with both interpretations, but the large size of this structure and its relationship to nearby active and inactive faults support the latter interpretation, as discussed below.

The geological map in Fig. 2 shows that the large anticline of this study makes up the northern half of an even larger, doubly plunging anticline located east of the Cañon Rojo fault. The southern part of this anticline is complicated by numerous smaller fault offsets and minor folds, but its overall geometry reveals a large composite anticline cored by the Imperial Formation (Fig. 2; Vázquez-Hernández, 1996; Vázquez-Hernández *et al*., 1996). This fold is a major structural element in the upper plate of the now-inactive part of the Cañada David detachment fault (see 'Tectonic and geological setting', above). Its orientation, large size, occurrence within Plio-Pleistocene sedimentary rocks and location in the upper plate of the inactive portion of the Cañada David detachment (Fig. 2) all suggest that its origin is probably related to slip on the underlying detachment fault. For these reasons we favour an interpretation in which the growth anticline formed as an extensional fault-bend fold produced by slip of the upper plate over a large bend in the underlying detachment fault during deposition of the redbeds sequence (Fig. 10).

Transtensional detachment faulting

The preceding interpretation of extensional fold origin leads us to conclude that deposition of the redbeds sequence took place in a supradetachment basin above the northern, now inactive part of the Cañada David detachment fault. According to this model, the basin was divided into two main subbasins by a large fault-bend fold that was created by slip over a bend in the underlying detachment fault. The presence of tonalitic, coarse-

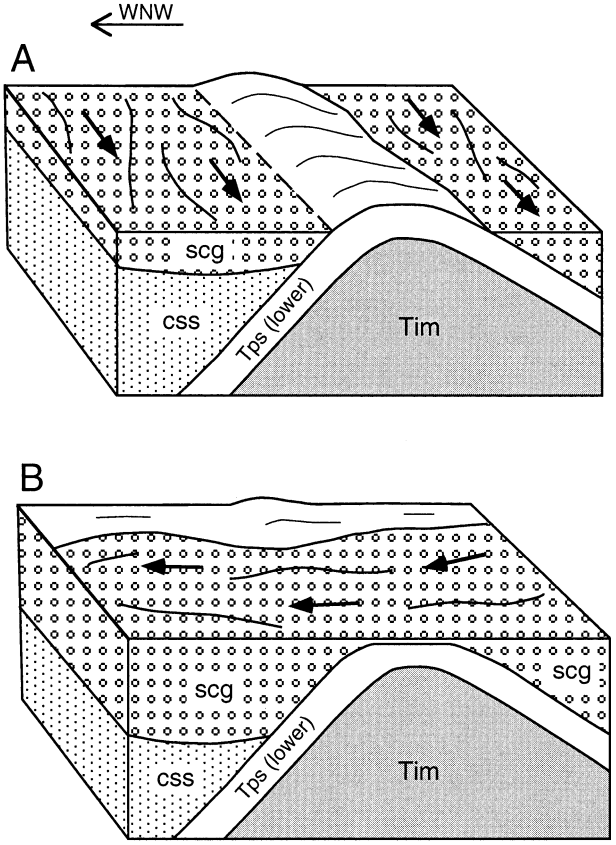

Fig. 11. Schematic diagrams showing structural interpretation for upsection change in palaeocurrent directions in conglomerate that progressively filled growth syncline on west flank of the growth anticline. See Figure 9D,E for palaeocurrent data and location; position in structural model is shown in Fig. 10. A. Early in gravel deposition sediment was funnelled to the SSW along axis of the actively growing syncline. B. Later the rate of fold growth slowed, or rate of gravel aggradation increased, causing sediment to fill the syncline and permitting transport across the axis of the buried structure. css = conglomeratic sandstone, scg = sandy conglomerate.

grained detritus in north-easterly derived steep alluvial fans indicates that the dextral-normal Laguna Salada fault was active during this phase of basin development and must have formed the faulted north-eastern margin of the basin. This indicates that the two faults were coeval and kinematically linked during deposition of the Plio-Pleistocene redbeds sequence and together accommodated transtensional strain during that time. Gravel and coarse sand in the redbeds and grey gravel consist exclusively of tonalitic detritus shed from the north-east side of the Laguna Salada fault, and there is no sign of input from metamorphic rocks now exposed in the footwall of the Cañada David detachment. This suggests that topographic relief in the footwall of the detachment fault was subdued and that high topography in the footwall of the Laguna Salada fault supplied most or all of the detritus to the basin.

The unconformity between the redbeds sequence and overlying Pleistocene grey gravel unit records erosion of rocks in the footwall of the Cañon Rojo fault followed by deposition of at least 600 m of gravel. Since then, slip on the Cañon Rojo fault has produced rapid uplift and erosion of footwall stratigraphy. From the above analysis it appears that the present phase of uplift was initiated when the northern part of the Cañada David detachment fault became inactive and slip was transferred to the Cañon Rojo fault. This sequence of basinward fault migration and resulting uplift of previously buried stratigraphy is similar to that described for other rift and supradetachment basins (Dart *et al.*, 1995; Horton & Schmitt, 1998; Knott, 1998). The erosional unconformity at the base of the grey gravel unit and the thick section of gravel above it suggest that initiation of slip on the Cañon Rojo fault and termination of the Cañada David detachment fault may have been episodic. Thus the grey gravel unit may record a sequence of events in which the position of the major normal fault in this area alternated between the Cañada David detachment and Cañon Rojo faults, concluding when the northern part of the Cañada David detachment was permanently abandoned and slip became established on the Cañon Rojo fault (Fig. 2).

In this analysis we view the Cañada David detachment and Laguna Salada fault as kinematically linked, coevolving structures that accommodated transtensional strain during Pliocene–Pleistocene time, consistent with recent recognition of the youthful age of detachment faulting in the area (Axen & Fletcher, 1998; Axen *et al.*, 1998, 1999). Later abandonment of the northern strand of the Cañada David detachment fault and initiation of the Cañon Rojo fault in middle or late Pleistocene time could be interpreted as representing either: (1) north-westward stepping of the breakaway by formation of a secondary breakaway in a NW-migrating detachment fault system (e.g. Spencer, 1984; Dorsey & Becker, 1995), or (2) south-eastward migrating change from extension-driven to strike-slip-driven transtensional faulting along the north-east margin of Laguna Salada. The latter interpretation is supported by the observation that in the northern part of the Laguna Salada basin the modern lacustrine depocentre and topographic low point are juxtaposed directly against the Laguna Salada and Cañon Rojo faults, whereas in the southern part of the basin the low point is located much further ($\approx$5–8 km) west of the active detachment fault (Fig. 2; Axen *et al.*, 1999). This comparison suggests that the northern part of the modern Laguna Salada basin is subsiding on steep oblique-slip and normal faults that produce large vertical displacements, while the southern part of the basin is bounded by a low-angle detachment fault that produces a significant horizontal component of slip, displacing the basin's topographic low point a large distance away from the surface trace of the detachment fault (e.g. Friedmann & Burbank, 1995). Additional study of active range-bounding normal faults (RF, Fig. 2) between the south end of the Cañon Rojo fault and the now inactive trace of the Cañada David detachment would be needed to help determine which of the above interpretations best

explains the ongoing evolution of faulting along the north-eastern margin of the Laguna Salada basin.

CONCLUSIONS

Pliocene–Pleistocene sedimentary rocks exposed in the footwall of the Cañon Rojo fault accumulated near the strike-slip margin of a transtensional supradetachment basin that formed in the upper plate of the top-to-the-west Cañada David detachment fault. Strata of the redbeds sequence display rapid lateral transitions from (1) boulder conglomerate and breccia facies that accumulated in steep alluvial fans shed from the uplifted footwall of the oblique-slip Laguna Salada fault, through (2) sandstone and conglomerate of a low-gradient alluvial fan system that traversed north-westward across the supradetachment basin, into (3) fine-grained sandstone and mudstone of the ancestral Colorado River. Synbasinal growth of a large anticline was produced by slip of the upper plate over a large bend in the detachment fault, and subsidence in the flanking syncline produced a local depocentre that accumulated more than 1000 m of alluvial stratigraphy near the Laguna Salada fault. In middle or late Pleistocene time the Cañada David detachment fault was abandoned and normal fault slip was transferred $\approx$10 km to the north-west, initiating rapid uplift and erosion of previously buried stratigraphy in the footwall of the Cañon Rojo fault. The strike-slip component of transtensional strain in this setting is produced by dextral-oblique slip on the Laguna Salada fault, which has been active and kinematically linked with the Cañada David detachment fault from Pliocene time to the present.

ACKNOWLEDGEMENTS

This research was conducted during a sabbatical leave of Rebecca Dorsey at Cicese that was supported by conacyt project 3250-T9308 to Gary Axen and Arturo Martin. Additional support of the field work was provided by the petroleum research fund of the American Chemical Society. Rodrigo Flores is thanked for his assistance in the field. We appreciate many insightful conversations about this work with John Fletcher and Gary Axen. This paper benefited from reviews of an earlier version of the manuscript by Susanne Janecke and Rob Gawthorpe.

REFERENCES

Axen, G.J. & Fletcher, J.M. (1998) Late Miocene-Pleistocene extensional faulting, northern Gulf of California, Mexico and Salton Trough, California. *Internat. Geol. Review*, **40,** 217–244.

Axen, G.J., Fletcher, J.M., Cowgill, E., Murphy, M., Kapp, P., MacMillan, I., Ramos-Velazquez, E. & Aranda-Gomez, J. (1999) Range-front fault scarps of the Sierra El Mayor, Baja California; formed above an active low-angle normal fault? *Geology*, **27,** 247–250.

Axen, G.J., Fletcher, J.F. & Martín-Barajas, A. (1998) Late Miocene-Pleistocene detachment faulting in the northern Gulf of California and western Salton Trough and its role in evolution of the Pacific-North America plate boundary. In: *Geol. Soc. Am. Cordillerna Section Guidebook, California State University Long Beach, Department of Geological Sciences, Field Trip #6* (Ed. by R.J. Behl).

Blair, T.C. (1987) Sedimentary processes, vertical stratification sequences, and geomorphology of the Roaring River alluvial fan, Rocky Mountain National Park, Colorado. *J. Sedim. Petrol.*, **57,** 1–18.

Blair, T.C. & McPherson, J.G. (1994) Alluvial fans and their natural distinction from rivers based on morphology, hydraulic processes, sedimentary processes, and facies assemblages. *J. Sedim. Res.*, **64,** 450–489.

Bull, W.B. (1972) Recognition of alluvial-fan deposits in the stratigraphic record. In: *Recognition of Ancient Sedimentary Environments* (Ed. by J.K. Rigby, & W.K. Hamblin), *SEPM Spec. Publ.*, **16,** 63–83.

Burbank, D., Meigs, A. & Brozovic, N. (1996) Interactions of growing folds and coeval depositional systems. *Basin Res.*, **8,** 199–223.

Burchfiel, B.C., Hodges, K.V. & Royden, L.H. (1987) Geology of Panamint Valley-Saline Valley pull-apart system, California; palinspastic evidence for low-angle geometry of a Neogene range-bounding fault. *J. Geophys. Res., B*, **92,** 10 422–10 410 426.

Burchfiel, B.C., Molnar, P., Zhang, P., Deng, Q., Zhang, W. & Wang, Y. (1995) Example of a supradetachment basin within a pull-apart tectonic setting: Mormon Point, Death Valley, California. *Basin Res.*, **7,** 199–214.

Christie-Blick, N. & Biddle, K.T. (1985) Deformation and basin formation along strike slip faults. In: *Strike-Slip Deformation, Basin Formation, and Sedimentation* (Ed. by K.T. Biddle & N. Christie-Blick), *SEPM Spec. Publ.*, **37,** 1–34.

Collinson, J.D. (1986) Alluvial sediments. In: *Sedimentary Environments and Facies* (Ed. by H.G. Reading), pp. 20–62. Blackwell Scientific, Oxford.

Crowell, J.C. & Link, M.H. (1982) *Geologic History of the Ridge Basin*. Pacific Section SEPM.

Dart, C., Cohen, H.A., Serdar Akyuz, H. & Barka, A. (1995) Basinward migration of rift-border faults; implications for facies distributions and preservation potential. *Geology*, **23,** 69–72.

Dibblee, T.W. Jr (1984) Stratigraphy and tectonics of the San Felipe Hills, Borrego Badlands, Superstition Hills, and vicinity. In: *The Imperial Basin–Tectonics, Sedimentation, and Thermal Aspects* (Ed. by C. A. Rigsby), *Los Angeles, California, Pacific Section SEPM*, **40,** 31–44.

Dinter, D.A. & Royden, L. (1993) Late Cenozoic extension in northeastern Greece: Strymon Valley detachment system and Rhodope metamorphic core complex. *Geology*, **21,** 45–48.

Dorsey, R.J. & Becker, U. (1995) Evolution of a large Miocene growth structure in the upper plate of the Whipple detachment fault, northeastern Whipple Mountains, California. *Basin Res.*, **7,** 151–163.

Ford, M., Williams, E.A., Artoni, A., Verges, J. & Hardy, S. (1997) Progressive evolution of a fault-related fold pair from growth strata geometries, Sant Llorenc de Morunys, SE Pyrenees. *J. Struct. Geol.*, **19,** 413–441.

Friedmann, S.J. & Burbank, D.W. (1995) Rift basins and supradetachment basins: Intracontinental extensional end-members. *Basin Res.*, **7,** 109–127.

Frostick, L.E. & Steel, R.J. (Eds) (1993) Tectonic signatures in sedimentary basin fills: an overview. In: *Tectonic Controls*

and Signatures in Sedimentary Successions, International Association of Sedimentologists, Special Publication, **20,** 1–9.

Gastil, R.G. & Fenby, S.S. (1991) Detachment faulting as a mechanism for tectonically filling the Gulf of California during dilation. In: *The Gulf and Peninsular Province of the Californias* (Ed. by. J.P. Dauphin & B.R.T. Simoneit), *Am. Ass. Petr. Geol., Memoir*, **47,** 371–376.

Gawthorpe, R.L., Sharp, I., Underhill, J.R. & Gupta, S. (1997) Linked sequence stratigraphic and structural evolution of propagating normal faults. *Geology*, **25,** 795–798.

Groshong, R.H. (1989) Half-graben structures; balanced models of extensional fault-bend folds. *Bull. Geol. Soc. Am.*, **101,** 96–105.

Gupta, S., Underhill, J., Sharp, I. & Gawthorpe, R. (1999) Role of fault interactions in controlling synrift sediment dispersal patterns: Miocene, Abu Alaqa Group, Suez Rift, Sinai, Egypt. *Basin Res.*, **11,** 167–190.

Hardy, S. & Poblet, J. (1994) Geometric and numerical model of progressive limb rotation in detachment folds. *Geology*, **22,** 371–374.

Horton, B.K. & Schmitt, J.G. (1998) Development and exhumation of a Neogene sedimentary basin during extension, east-central Nevada. *Bull. Geol. Soc. Am.*, **110,** 163–172.

Janecke, S.U., Vandenburg, C.J. & Blankenau, J.J. (1998) Geometry, mechanisms and significance of extensional folds from examples in the Rocky Mountain Basin and Range Province, U.S.A. *J. Struct. Geol.*, **20,** 841–856.

Knott, J.R. (1998) Late Cenozoic tephrochronology, stratigraphy, geomorphology, and neotectonics of the western Black Mountains piedmont, Death Valley, California: Implications for the spatial and temporal evolution of the Death Valley fault zone. PhD Thesis, University of California, Riverside.

Leeder, M.R. & Gawthorpe, R.L. (1987) Sedimentary models for extensional tilt-block/half-graben basins. In: *Continental Extensional Tectonics* (Ed. by. M. P.Coward, J. F. Dewey & P. L. Hancock), *Geol. Soc. London Spec. Publ.*, **28,** 139–152.

Mann, P. (1997) Model for the formation of large, transtensional basins in zones of tectonic escape. *Geology*, **25,** 211–214.

May, S.R., Ehmen, K.D., Gray, G.G. & Crowell, J.C. (1993) A new angle on the tectonic evolution of the Ridge basin, a 'strike-slip' basin in southern California. *Geol. Soc. Am. Bull.*, **105,** 1357–1372.

McClay, K.R. & Scott, A.D. (1991) Experimental models of hangingwall deformation in ramp-flat listric extensional fault systems. *Tectonophysics*, **188,** 85–96.

Mueller, K.J. & Rockwell, T.K. (1991) Late Quaternary structural evolution of the western margin of the Sierra Cucapa, northern Baja California. In: *The Gulf and Peninsular Province of the Californias* (Ed. by. J.P. Dauphin & B.R.T. Simoneit), *Am. Ass. Petr. Geol., Memoir*, **47,** 249–260.

Mueller, K.J. & Rockwell, T.K. (1995) Late Quaternary activity of the Laguna Salada Fault in northern Baja California, Mexico. *Bull. Geol. Soc. Am.*, **107,** 8–18.

Oldow, J.S., Kohler, G. & Donelick, R.A. (1994) Late Cenozoic extensional transfer in the Walker Lane strike-slip belt, Nevada. *Geology*, **22,** 637–640.

Reineck, H.E. & Singh, I.B. (1980) *Depositional Sedimentary Environments*. Springer-Verlag, Berlin.

Rust, B.R. & Koster, E.H. (1984) Coarse alluvial deposits. In: *Facies Models*, 2nd edn (Ed. by R.G. Walker), pp. 53–69. Geol. Assoc. Can., Toronto.

Schlische, R.W. (1995) Geometry and origin of fault-related folds in extensional settings. *Bull. Am. Ass. Petr. Geol.*, **79,** 1661–1678.

Siem, M.E. & Gastil, R.G. (1994) Mid-Tertiary to Holocene extension associated with the development of the Sierra El Mayor metamorphic core complex, notheastern Baja California, Mexico. In: *Geological Investigations of an Active Margin* (Ed. by S.F. McGill & T.M. Ross), pp. 107–119. Geological Society of America Cordillerna Section Guidebook, Redlands, California, San Bernadino County Museum Association.

Spencer, J.E. (1984) Role of tectonic denudation in warping and uplift of low-angle normal faults. *Geology*, **12,** 95–98.

Suppe, J., Sabat, F., Munoz, J.A., Poblet, J., Roca, E. & Verges, J. (1997) Bed-by-bed fold growth by kink-band migration; Sant Llorenc de Morunys, eastern Pyrenees. *J. Struct. Geol.*, **19,** 443–461.

Tankard, A.J., Welsink, H.J. & Jenkins, W.A. (1989) Structural styles and stratigraphy of the Jeanne d'Arc Basin, Grand Banks of Newfundland. In: *Extensional Tectonics and Stratigraphy of the North Atlantic Margins* (Ed. by A.J. Tankard & H.R. Balkwill), *Am. Ass. Petr. Geol., Memoir*, **46,** 265–282.

Vázquez-Hernández, S. (1996) Estratigrafia y ambientes de depositos de la secuencia sedimentaria al oriente de Laguna Salada, Baja California. Master Thesis, Centro de Investigacion Cientifica y Educacion Superior de Ensenada, Ensenada Baja California.

Vázquez-Hernández, S., Carreño, A.L. & Martín-Barajas, A. (1996) Stratigraphy and paleoenvironments of the Mio-Pliocene Imperial Formation in the eastern Laguna Salada area, Baja California, Mexico. In: *American Association of Petroleum Geologists Field Conference Guide* (Ed. by P. Abbott & J. Cooper), *Pacific Section SEPM*, **80,** 373–380.

Wells, S.G. & Harvey, A.M. (1987) Sedimentologic and geomorphologic variations in storm-generated alluvial fans, Howgill Fells, northwest England. *Bull. Geol. Soc. Am.*, **98,** 182–198.

Winker, C.D. (1987) Neogene stratigraphy of the Fish Creek-Vallecito section, Southern California; implications for early history of the northern Gulf of California and Colorado Delta. PhD Thesis, University of Arizona, Tucson.

Winker, C.D. & Kidwell, S.M. (1996) Stratigraphy of a marine rift basin: Neogene of the western Salton Trough. In: *Field Conference Guidebook and, Vol. For the Annual Convention, San Diego, California, May, 1996* (Ed. by P.L. Abbott & J.D. Cooper), *Pacific Section Am. Ass. Petr. Geol.*, **73,** 295–336.

Withjack, M.O., Olson, J. & Peterson, E. (1990) Experimental models of extensional forced folds. *Bull. Am. Ass. Petr. Geol.*, **74,** 1038–1054.

Woodward, G.D. (1974) Redefinition of the Cenozoic stratigraphic column in Split Mountain Gorge, Imperial Valley, California. *Bull. Am. Ass. Petr. Geol.*, **58,** 521–526.

Xiao, H. & Suppe, J. (1992) Origin of rollover. *Bull. Am. Ass. Petr. Geol.*, **76,** 509–529.

Received 29 October 1998; revision accepted 18 June 1999